Fuel Cells DOI: 10.1002/fuce.200400075

Advances in Mixed-Reactant Fuel Cells

A. K. Shukla[1,2], R. K. Raman[1], and K. Scott[3]*

[1] Solid State and Structural Chemistry Unit, Indian Institute of Science, Bangalore-560 012, India
[2] Central Electrochemical Research Institute, Karaikudi-630 006, India
[3] School of Chemical Engineering and Advanced Materials, Merz Court, University of Newcastle, Newcastle upon Tyne, NE1 7RU, UK

Received March 5, 2004; accepted November 20, 2004

Abstract

The mixed-reactant fuel cell (MRFC) is a new concept, in which a mixture of aqueous fuel and gaseous oxygen (or air) flows directly through a porous anode-electrolyte-cathode structure or through a strip-cell with an anode-electrolyte-cathode configuration. These structures can be single cells or parallel stacks of cells and may be in a planar, tubular or any other geometry. Selectivity in the electrocatalysts for MRFCs is mandatory to minimize mixed-potential at the electrodes, which otherwise would reduce the available cell voltage and compromise the fuel efficiency. MRFC offers a cost effective solution in fuel cell design, since there is no need for gas-tight structure within the stack and, as a consequence, considerable reduction in sealing, manifolding and reactants delivery structure is possible. In recent years, significant advances have been made in MRFCs, using methanol as a fuel. This paper reviews the status of mixed reactant fuel cells and reports some recent experimental data for methanol fuel cell systems.

Keywords: DMFC, Fuel Cell, Mixed Flow, Mixed Reactant, Selective Electrocatalyst

1 Introduction

Fuel cells are chemoelectric engines, which convert the chemical energy of a fuel directly into electricity. The process is an electrochemical reaction akin to a battery. Unlike the battery, fuel cells do not store the energy within the chemicals internally, but instead use a continuous supply of fuel from an external storage tank. Accordingly, fuel cell systems have the potential to solve the most challenging problems associated with the currently available battery systems, namely insufficient energy at a given weight (specific energy density) or volume (volumetric energy density). Besides, while leading battery technologies are reaching their practical energy storage capabilities, commercial fuel cells are still in their infancy. Furthermore, in comparison to simple combustion of the fuel, since fuel cells operate without a thermal cycle, they offer a radical increase in energy efficiency and also virtual elimination of air pollution without the use of emission control devices as in conventional energy conversion [1–3].

A fuel cell consists of two electrodes; an anode to which the fuel is supplied and a cathode to which the oxidant is supplied, and the electrolyte which separates the two electrodes and allows ions to flow between them. There are six generic types of fuel cells in various stages of development, namely (i) phosphoric acid fuel cells (PAFCs), (ii) alkaline fuel cells (AFCs), (iii) polymer electrolyte fuel cells (PEFCs), (iv) molten electrolyte fuel cells (MCFCs), (v) solid oxide fuel cells (SOFCs), and (vi) direct methanol fuel cells (DMFCs). The most advanced fuel cells in terms of applications and commercialization are AFCs, used successfully in space programs in the mid 1960s and PAFCs used for stationary power plants. These fuel cells were also originally intended to power electric vehicles but AFCs are very sensitive to electrolyte carbonation due to the presence of carbon dioxide either in a reformate hydrogen fuel or in the atmosphere. The PAFCs are rather complex, too heavy and bulky, to fit into an engine compartment of a car. An alternative fuel cell, the PEFC offers low-operating temperature and rapid start-up characteristics together with a robust solid-state construction which gives it a clear advantage for application in cars [4]. The preferred fuel for PEFCs is hydrogen and while many strategies for providing hydrogen to PEFCs are being evaluated, the most acceptable option appears to be to generate hydrogen onboard and on-demand from liquid hydrocarbons or methanol [5]. A technical challenge however lies in modifying large-scale industrial steam-reforming or partial-oxidation reactors to lightweight units that can fit inside the car. An elegant solution to the problems associated with the need for gaseous hydrogen fuel, lies in operating the PEFCs directly with a liquid fuel. Substantial efforts are therefore being expended on PEFCs that run on air plus a mixture of methanol and water [6–10]. A solid-polymer-electrolyte direct methanol fuel cell (SPE-DMFC) would be about as efficient as

[*] *Corresponding author, k.scott@ncl.ac.uk*

a conventional reformer-based PEFC unit, in both its construction and operation. Although substantial improvements have been made in the power efficiencies of conventional direct methanol fuel cells (CDMFCs) since their inception, it would be mandatory to make these cost-effective for their commercial viability. One such effort in this direction is the development of mixed-reactant direct methanol fuel cells (MR- DMFCs) [6–10]. Clearly methanol is not the only fuel that could be potentially used in MRFCs although much of the effort in this direction has been with methanol. This article reviews the advances made in MRFCs, and particularly MRDMFCs.

1.1 Mixed Reactant Fuel Cells

One of the first reported mixed-reactant fuel cells used a liquid reactant mixture of methanol and hydrogen peroxide in an alkaline solution [11]. The tests were conducted on a stack of 40 cells using bipolar electrodes with Pt anode and Ag cathode. The stack delivered power at 40 A and 15 V and although was not particularly efficient, it clearly demonstrated the concept of a MR-DMFC. The performance was not as good as that from a separated fuel and oxidant fuel cell as indicated in open cell potentials of 0.41 V for MR-DMFC against 0.81 V for standard configurations. Another reason for possible inferior performance of the MR-DMFC is due to current leakage or bypass losses in the cell stack.

Barton et al. demonstrated the MR-DMFC concept using a strip electrode configuration which was fed with a two phase mixture of methanol solution and air [6]. The cell used Pt-Ru/C anode catalysts and tetramethoxyphenyl porphyrin or RuSeMo/C cathode catalysts. Both of the cathode catalysts exhibited good methanol tolerance for oxygen reduction. The mixed reactant mode cell gave slightly better performance than the standard separated-fuel and oxidant system.

The history of mixed-reactant fuel cell goes back to the 1950's in which tests were performed on mixed hydrogen and air systems. The cells were based on an alkaline electrolyte and used "selective" cathode catalysts of C, Au or Ag, materials that are not good hydrogen oxidation catalysts [12, 13]. The cells were operated in two modes, one in which the fuel and oxygen mixture were first fed to the cathode and then to the anode and the other in which the reactant mixtures were both fed simultaneously to the anode and cathode. Although open-circuit potentials of 1.0 V were obtained, on-load power performance was not impressive, 0.4 V at 4 mA cm^{-2}.

The use of mixed-reactant fuel cells based on hydrogen and oxygen using high temperature and thin film alumina electrolytes was suggested in 1965 with a strip cell design [14]. In the mid 1970's, the cell was experimentally tested using dilute hydrogen and air mixtures and achieved a peak power of 0.32 μW cm^{-2} at a voltage of 0.39 V [15]. More recent reports of high temperature solid oxide fuel cells operating on mixed reactants have been made by Dyer et al. [16] and Hibino and Iwahara [17], and the subject was reviewed in 1995 [18]. A solid oxide fuel cell (SOFC) with a mixed methane and air feed has been reported [19], and a low operating temperature solid oxide fuel cell using a hydrocarbon-air mixture and a samaria-doped ceria electrolyte has been reported [20]. The use of a strip cell design for mixed reactant SOFC systems has also been reported [21, 22]. In the solid oxide systems, the power densities generated by the mixed reactant cells have been quite respectable. Hibino et al. for example achieved 166 mW cm^{-2} using $BaCe_{0.8}Y_{0.2}O_{3-a}$ electrolyte at 950 °C with a Pt anode and Au cathode [23]. In a later study using ethane and air at 500 °C, and a $Ce_{0.8}Sm_{0.2}O_{1.9}$ electrolyte for example, a peak power density of 400 mW cm^{-2} at 0.5 V has been demonstrated [20, 24].

Although there has been some significant effort in the development of mixed reactant fuel cells with hydrogen and hydrocarbon fuels and some very respectable power performances are achieved, there is inevitably concern over the use of an explosive mixture within a cell where the potential for electrical spark ignition is real. Thus mixed reactant cells will probably need to operate outside the explosive ranges of fuel and air mixtures and use dilute fuel mixtures. One such example is the mixed-reactant direct methanol fuel cell, which operates well on dilute fuel compositions in the presence of water.

2 Operating Principle of MR-DMFCs

In a fuel cell employing an acid electrolyte, methanol can be directly oxidized to carbon dioxide at the anode according to the reaction,

$$CH_3OH + H_2O \rightarrow CO_2 \uparrow + 6H^+ + 6e^- \quad (1)$$

The thermodynamic potential ($E°_a$) for Eq. (1) calculated from the standard chemical potentials at 25 °C is 0.02 V *vs.* SHE. At the cathode, oxygen gas combines concomitantly with the protons and electrons and is reduced to water through the reaction,

$$3/2O_2 + 6H^+ + 6e^- \rightarrow 3H_2O \quad (2)$$

The thermodynamic potential ($E°_C$) for Eq. (2) is 1.23 V *vs.* SHE. Accordingly, the net cell reaction is represented as,

$$CH_3OH + 3/2O_2 \rightarrow 2H_2O + CO_2 \uparrow \quad (3)$$

Accordingly, the standard electromotive force (e.m.f.), $E°_{eq}$ = 1.21 V. In practice, the operating cell potential at reasonable current densities is 0.5 V and the potential efficiency of a DMFC is approximately 40%. The specific energy density for methanol is $-\Delta G°/(3{,}600 \times M) = (702 \times 10^3) / (3{,}600 \times 0.032)$ = 6.1 kWh kg^{-1}, where M is the molecular weight of methanol.

The direct electro-oxidation of methanol in a fuel cell has been the subject of study for more than three decades. The early cell designs utilized aqueous sulphuric acid electrolyte

at 60 °C. About 20 years ago, Shell Research Centre in the UK and Hitachi Research Laboratories in Japan built DMFC stacks of up to 5 kW but their power densities were only 20–30 mW cm^{-2} even with platinum loadings as high as 10 mg cm^{-2}, which corresponds to specific power densities of 2–3 W g^{-1} of platinum catalysts.

A major drawback of the DMFC is the very sluggish anode reaction, which coupled with the inefficient cathode reaction, gives rise to the relatively low overall performance, particularly at low temperatures. The performance of the cells utilizing sulphuric acid electrolyte is further limited due to the high internal resistance of the system. In the 1980s, it was realized that a considerable increase in the efficiency might be obtained by using the 'zero gap' cell design principle in which the liquid electrolyte is replaced by a thin proton-conducting polymer sheet such as Nafion® – a perfluoro-sulphonic acid polymer [25] made by DuPont. A DMFC with a Nafion® electrolyte membrane is shown schematically in Figure 1. In a SPE-DMFC, methanol dissolved in water is supplied to an anode, but the methanol has the tendency to pass through the membrane electrolyte (crossover) and hence affect the performance of the cathode [26–28]. Therefore, a fundamental limitation in the practical realization of such a SPE-DMFC has been the existence of electrochemical losses at both the anode and the cathode, arising mainly due to the electrocatalytic restrictions and methanol crossover through the electrolyte membrane, caused by diffusion and osmotic drag. The polarization curve for a DMFC along with its constituent electrodes is shown in Figure 2. In this figure, we see

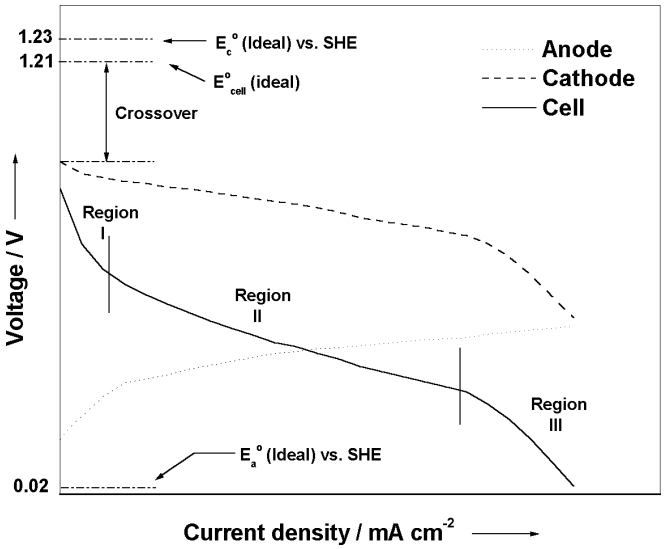

Fig. 2 Schematic polarization curve for a CDMFC and its constituent electrodes.

that the major losses in potential are both at the anode and the cathode. To try to minimize the potential losses due to methanol crossover several research groups have been developing selective cathode catalysts, which are methanol tolerant [6–10]. From the development of methanol tolerant cathode catalysts, the concept of mixed reactant fuel cells can then be broached.

In a MR-DMFC, the fuel and the oxidant are allowed to mix together before feeding to the fuel cell [6–8]. Such a situa-

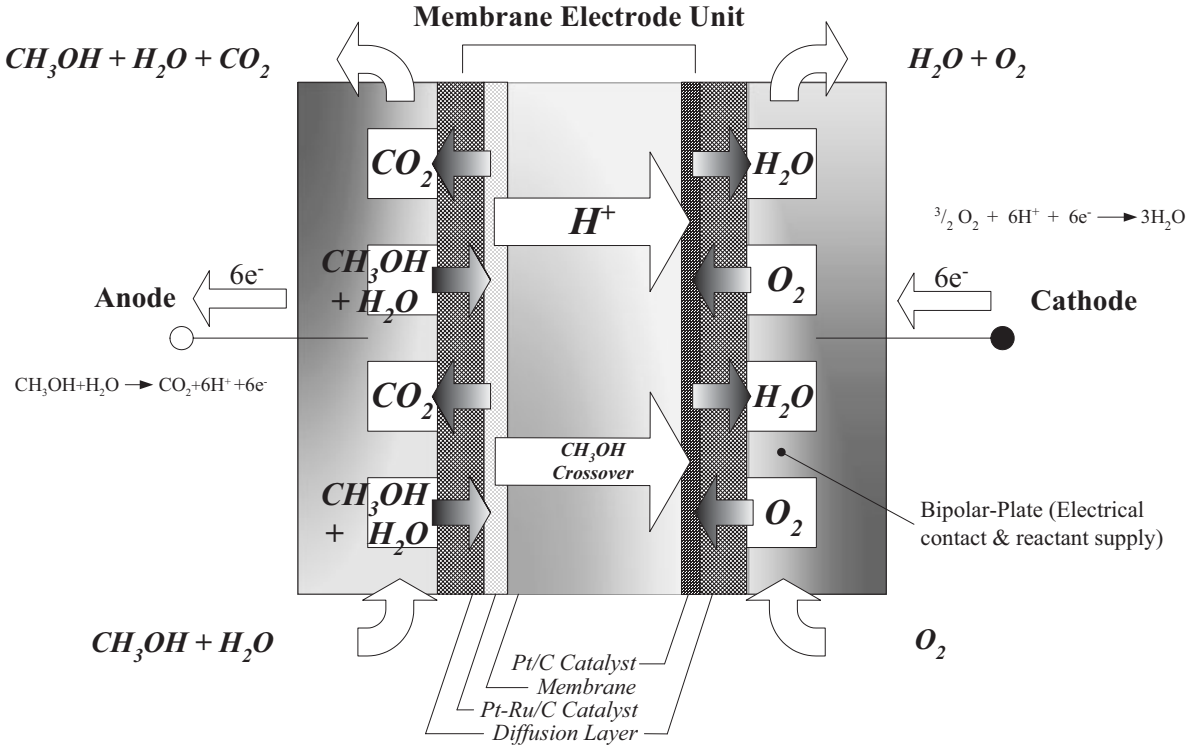

Fig. 1 Schematic diagram of a CDMFC.

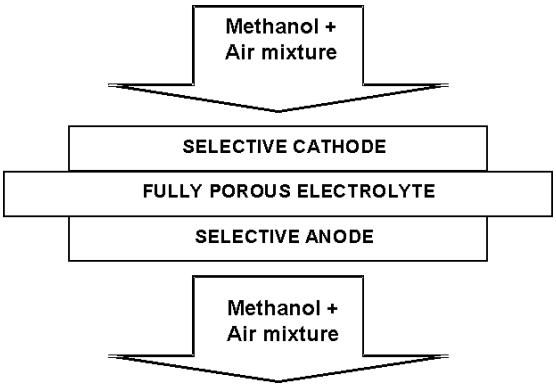

Fig. 3 Schematic diagram of a MR-DMFC stack.

tion avoids the need for a gas-tight structure within the stack and provides relaxation for sealing the reactants/products delivery structure (Figure 3). As a consequence, the cost of the cell can be much lower than in standard cell systems. However, it is mandatory to employ selective catalysts for methanol oxidation and oxygen reduction in MR-DMFCs [6–10]. The various advantages and disadvantages of MR-DMFCs are given in Table 1.

Table 1 Advantages and disadvantages of MR-DMFCs.

Advantages	Disadvantages
(i) No need for gas-tight structure within the stack providing relaxation of sealing the reactant/products delivery structures.	(i) Selective electrocatalysts mandatory.
(ii) Simplified manifolding.	(ii) High ohmic resistance between the neighboring cells, when a strip-electrode configuration is used.
(iii) Cheaper than conventional fuel cells.	(iii) Crossover inevitable.

3 Selective Electrocatalysts for MR-DMFCs

Various selective electrocatalysts being employed in MR-DMFCs both for the anodic oxidation of methanol and the cathodic reduction of oxygen are briefly described in this section.

3.1 Selective Catalysts for Anodic Oxidation of Methanol

Several reaction mechanisms have been proposed for the anodic oxidation of methanol. Broadly speaking, the basic mechanism for methanol oxidation can be summarized in two functionalities, namely the electrosorption of methanol on to the substrate followed by addition of oxygen to adsorb carbon-containing intermediates to generate carbon dioxide.

In practice, only a few electrode materials are capable for adsorption of methanol. In acidic media, only platinum [29] and platinum-based catalysts [30–32] have been found to show sensible activity, and almost all mechanistic studies have concentrated on these materials. On platinum itself, adsorption of methanol is believed to take place through a sequence of steps described below [29].

The first step is dissociative chemisorption of methanol onto the platinum surface, which involves successive donation of electrons to the catalyst as follows.

$$Pt + CH_3OH \xrightarrow{k_1} Pt\text{-}CH_2OH + H^+ + e^- \quad (4)$$

$$Pt + Pt\text{-}CH_2OH \xrightarrow{k_2} Pt_2\text{-}CHOH + H^+ + e^- \quad (5)$$

$$Pt + Pt_2\text{-}CHOH \xrightarrow{k_3} Pt_3\text{-}COH + H^+ + e^- \quad (6)$$

Here $k_1 < k_2 < k_3$ makes Pt_3-COH as the major surface species. A surface rearrangement of the oxidation intermediates generates carbon monoxide, linearly or bridge-bonded to Pt-sites according to the reaction,

$$Pt_3\text{-}COH \rightarrow Pt_3\text{-}CO + H^+ + e^- \quad (7)$$

Water discharge occurs at high anodic overpotentials on Pt with the formation of Pt-OH species at the platinum surface as shown below.

$$Pt + H_2O \rightarrow Pt\text{-}OH + H^+ + e^- \quad (8)$$

The ultimate step is the reaction of Pt-OH groups with neighboring methanolic residues to give carbon dioxide according to the following reaction.

$$Pt\text{-}OH + Pt_3\text{-}CO \rightarrow 4Pt + CO_2 \uparrow + H^+ + e^- \quad (9)$$

Accordingly, the overall oxidation of methanol to carbon dioxide proceeds through a six-electron donation process. In the literature, it has been documented that methanol can also be oxidized directly to CO_2 without being first adsorbed as CO; this has been referred to as duel pathway mechanism [33].

Platinum alone is not sufficiently active for methanol oxidation and there is need for a promoter that effectively provides oxygen in some active form to achieve facile oxidation of chemisorbed CO on platinum. In the literature, various approaches towards platinum promotion have been attempted. The simplest method is to generate more Pt-O species on the platinum surface by incorporating certain metals with platinum to form alloys such as Pt_3Cr and Pt_3Sn, which then dissolve to leave highly reticulated but active surfaces. A second approach has been the use of surface adatoms produced by underpotential deposition on the platinum surface. A third type of promotion is the use of alloys of platinum with different metals such as Pt-Ru, Pt-Os, Pt-Ir, etc., where the second metal forms the surface oxide in the potential range for methanol oxidation. Among these, Pt-Ru alloy [29, 32] has been found to be particularly effective and efforts have been made to enhance the promotion on Pt-Ru based ternary, as well as quaternary alloys, namely Pt-Ru-Os and Pt-Ru-Ir, etc.

The fourth type of promotion described in the literature is a combination of Pt with a base-metal oxide such as Nb, Zr,

Ta, etc. In addition to electrodeposition or reductive deposition of Pt onto an oxide surface such as Pt-WO_3 [34], attempts have also been made to study methanol oxidation on pervoskite-based oxides with platinum, such as $SrRu_{0.5}Pt_{0.5}O_3$. It also appears that certain amorphous metal alloys, such as Ni-Zr, which form a thick passive oxyhydroxide film, could also facilitate methanol oxidation.

Among the various methanol oxidation catalysts described above, perhaps Pt-Ru and Pt-Sn are the most widely studied catalysts [29, 35, 36]. It has been shown that the alloying of Sn and Ru with Pt gives rise to electrocatalysts, which strongly promote the oxidation of methanol and related methanolic species. On the platinum surface, at low potentials –CO groups are adsorbed while at high potentials chemisorption of –OH groups takes place during the electro-oxidation of methanol with both the processes being distinctly separated. On a Pt-Ru surface, the chemisorption of –OH groups shifts to lower potentials and overlaps with the region where –CO groups are adsorbed on the catalyst as shown in Figure 4. On a Pt-Ru alloy, water discharging occurs on Ru-sites at much lower potentials in relation to pure Pt catalyst as depicted in Figure 4 according to the following reaction:

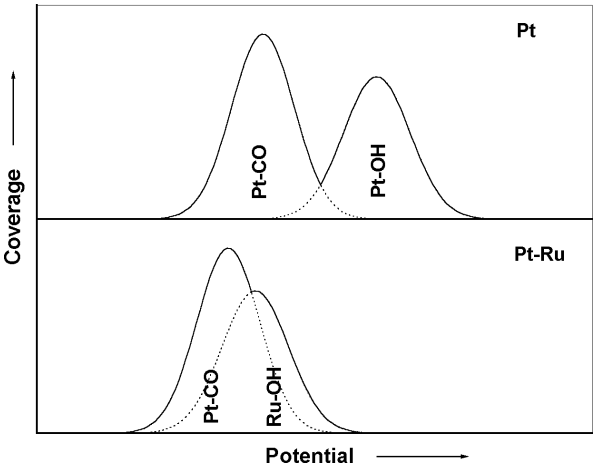

Fig. 4 Schematic description of -CO oxidation on Pt and Pt-Ru surface by M-OH group.

$$Ru + H_2O \rightarrow Ru\text{-}OH + H^+ + e^- \quad (10)$$

The final step is the reaction of Ru-OH groups with the neighbouring methanolic residues adsorbed on Pt to give carbon dioxide according to the reaction,

$$Ru\text{-}OH + Pt\text{-}CO \rightarrow Ru + Pt + CO_2 \uparrow + H^+ + e^- \quad (11)$$

The following reaction scheme has been envisaged for methanol oxidation on Pt-Sn alloy catalyst [35, 36].

$$Sn\text{-}Pt + CH_3OH \rightarrow Sn\text{-}(Pt\text{-}CHO) + 3H^+ + 3e^- \quad (12)$$

$$Sn\text{-}(Pt\text{-}CHO) + H_2O \rightarrow (Sn\text{-}OH)\text{-}(Pt\text{-}CHO) + H^+ + e^- \quad (13)$$

$$(Sn\text{-}OH)\text{-}(Pt\text{-}CHO) \rightarrow (Sn\text{-}OH)\text{-}(Pt\text{-}CO) + H^+ + e^- \quad (14)$$

$$(Sn\text{-}OH)\text{-}(Pt\text{-}CO) \rightarrow Sn\text{-}Pt + CO_2 \uparrow + H^+ + e^- \quad (15)$$

From the foregoing, one can conclude that the addition of Ru and Sn to Pt markedly promotes the electrocatalytic activity of Pt through the adsorption of oxygenated species on Ru or Sn sites. Obviously, methanol oxidation is more facile on Pt-Ru surfaces because the reaction desires the electrocatalyst to be used in potential regime where labile-bonded oxygen should be present on the surface. In this situation, the supply of active oxygen to the species is of paramount importance, since this, apparently, would facilitate the oxidation of adsorbed methanolic residues to carbon dioxide. It has been documented that with the Pt-Sn alloy catalyst, promotion of methanol oxidation is seen in the low-potential region while Pt-Ru is particularly active in the high potential region. The obvious catalyst promoter pair therefore would have been Sn and Ru, but Sn and Ru are not quite miscible, and attempts to form a ternary Pt-Ru-Sn alloy have led to expulsion of Ru.

A plausible explanation for selectivity of Pt-Ru catalyst towards methanol oxidation could be as follows. Methanol is preferentially chemisorbed on Pt-Ru surface in relation to oxygen. As a consequence, the availability of dioxygen to catalytic Pt-sites is restricted. Besides, oxygen, if any, will be attracted towards oxophilic Ru-sites in Pt-Ru keeping the catalytic Pt-sites active towards methanol oxidation.

To prepare active Pt-Ru/C and Pt-Sn/C catalysts the following procedures have been adopted. The desired amounts of $Na_6Pt(SO_3)_4$ and $Na_6Ru(SO_3)_4$ were dissolved in 1.0 M H_2SO_4 and diluted with distilled water [37], and the solution was added drop-wise to the distilled-water with constant stirring. Simultaneously, 30% H_2O_2 was added drop-wise to decompose the sulfito-complexes, which resulted in vigorous gas evolution. The solution was further stirred for 1 h at 80 °C to decompose excess H_2O_2. This step was followed by the addition of a Vulcan XC-72R carbon slurry. Subsequently, carbon-supported Pt-Ru was obtained by bubbling H_2 gas vigorously into the solution, which was filtered, washed copiously with hot distilled water, and dried in an air oven at 80 °C for 2 h.

In order to prepare Pt-Sn alloy catalyst [35, 36], a required amount of Vulcan XC-72R carbon is suspended in deionized water and agitated in an ultrasonic bath with constant stirring at 80 °C. Appropriate volumes of the solutions of chloroplatinic acid in water and tin chloride in dilute HCl are slowly added to the carbon suspension, under constant stirring, with the temperature maintained at about 80 °C. The resulting mass is left for 1.0 h, with constant stirring, to achieve complete impregnation of carbon with chloroplatinic acid and tin chloride solutions. This is followed by drop-wise addition of 0.2 M hydrazine solution, which is slightly higher than the stoichiometric amount required for complete reduction to Pt and Sn metals. Subsequently, 0.5 M NaOH solution is added to the slurry to bring the *pH* to near neutral. The slurry is then

filtered, copiously washed with hot distilled water and dried in an air oven.

3.2 Selective Electrocatalysts for Cathodic Reduction of Dioxygen

Cathodic oxygen-reduction can proceed by two different pathways, namely (i) the direct four-electron pathway, and (ii) the peroxide pathway. The direct four-electron pathway in an alkaline medium proceeds as,

$$O_2 + 2H_2O + 4e^- \rightarrow 4OH^- \ (E^\circ = 0.4 \text{ V } \textit{vs.} \text{ SHE}) \quad (16)$$

and in acidic medium as,

$$O_2 + 4H^+ + 4e^- \rightarrow 2H_2O \ (E^\circ = 1.23 \text{ V } \textit{vs.} \text{ SHE}) \quad (17)$$

The peroxide pathway in alkaline medium proceeds as,

$$O_2 + H_2O + 2e^- \rightarrow HO_2^- + OH^- \ (E^\circ = -0.07 \text{ V } \textit{vs.} \text{ SHE}) \quad (18)$$

followed by peroxide reduction to OH^- ions as,

$$HO_2^- + H_2O + 2e^- \rightarrow 3OH^- \ (E^\circ = 0.87 \text{ V } \textit{vs.} \text{ SHE}) \quad (19)$$

or, by chemical decomposition of peroxide as,

$$2HO_2^- \rightarrow 2OH^- + O_2 \quad (20)$$

In an acidic medium, production of dioxygen through the peroxide pathway is possible as follows:

$$O_2 + 2H^+ + 2e^- \rightarrow H_2O_2 \ (E^\circ = 0.67 \text{ V } \textit{vs.} \text{ SHE}) \quad (21)$$

This follows as either,

$$H_2O_2 + 2H^+ + 2e^- \rightarrow 2H_2O \ (E^\circ = 1.77 \text{ V } \textit{vs.} \text{ SHE}) \quad (22)$$

or,

$$2H_2O_2 \rightarrow 2H_2O + O_2 \quad (23)$$

The direct four-electron pathway does not involve the peroxide species and hence has a higher faradic efficiency in relation to the peroxide pathway [38]. However, it has proven difficult to find catalysts, which facilitate the direct four-electron pathway for dioxygen reduction.

As indicated in Section 2, in addition to irreversible losses, associated with the kinetics of oxygen reduction, there is an additional overpotential observed on the cathode owing to methanol crossover in a CDMFC [28]. Therefore, cathodes with high loadings of platinum are usually employed in CDMFCs [25]. However, since methanol has the tendency to be chemisorbed preferentially on platinum, it appears mandatory to develop both methanol impermeable membranes and methanol tolerant oxygen reduction catalysts for practical realization of CDMFCs. In recent years, certain Ru-based chalcogenides have shown promise as methanol-tolerant oxygen reduction catalysts [8, 9]. However, these materials have much lower intrinsic specific activity for oxygen reduction in relation to platinum.

In general, there are some four classes of oxygen-reduction electrocatalysts. The most familiar of these are the noble metals, particularly platinum, which has been extensively investigated both as pure metal [39], nanoparticle [40] and platinum metal alloys [39, 40–44], and as polycrystalline and single-crystal surfaces [45, 46]. Among various binary-alloys of transitional-metals with platinised carbon, Pt-Fe alloy catalyst has been reported as potential methanol-resistant oxygen-reduction catalysts [10]. A second class of electrocatalysts is made up of the macrocyclic derivatives of a wide range of transition-metal compounds [47]. The most investigated of these are cobalt and iron, and among the ligands studied, porphyrins, tetra-azaanulenes, and dimethyl glyoxime derivatives are well established [48–51].

A third class of catalysts is derived from metallic oxides [52]. Many oxides, particularly of the second and third-row transition elements, show metallic conductivity [53], usually derived from M-O-M bonding rather than direct M-M overlap to maximize d-orbital electron density at the Fermi level, and can therefore be fabricated into electrodes without addition of a conducting matrix. Particularly, in alkaline solution, a number of such oxides, including spinel [54], perovskite [55], and pyrochlore structures [56], show remarkable activity for oxygen reduction. But in acid solutions, the activity declines substantially, and the oxide phase is also less stable. Related to the oxides are members of the fourth class of electrocatalysts, which are based on transition-metal compounds with other non-metallic counter ions, derived from the chalcogenides [57–69]. The chalcogenides are frequently highly stable, especially in combination with later transition metals, and can be immersed in aqueous acids and held at high positive potentials without any appreciable degradation. Studies of compounds from this class have only taken place within the last ten years, but it is already clear that their activity toward oxygen reduction is remarkable. The preparatory methods for the above oxygen-reduction catalysts are briefly described below.

If either the particle size of platinum electrocatalyst for oxygen reduction is very small or the platinum electrocatalyst is amorphous, the methanol chemisorbtion energy should be lower and the cathode would be less susceptible to methanol chemisorption [4]. Accordingly, various preparatory routes have been proposed to synthesize platinum and platinum-alloy electrocatalysts with finer particle-sizes [70]. Among these, the most attractive procedure is due to Bonnemann et al. [71, 72]; here platinum dichloride ($PtCl_2$) is suspended in tetrahydrofuran (THF) and treated with tetra-alkyl ammonium hydro-tri-organoborate, which results in a platinum metal colloid solution with a minimal evolution of hydrogen. This colloidal solution is evaporated to dryness under high vacuum, and the resultant waxy residue is mixed with ether.

The colloid is then precipitated by addition of ethanol. The gray-black metal colloid powder thus obtained has a particle size between 1–5 nm. Maillard et al. [73] reported that the mass activity of platinum towards oxygen reduction increases continuously with a decrease in particle size from 4.6 to 2.3 nm, whereas mass activity is roughly independent of size in methanol-free electrolyte when the platinum particle size is less than 3.5 nm. The effects of adding second metal to platinum have also been investigated. Although both Pt-Co/C and Pt-Fe/C have been reported to be methanol-resistant oxygen-reduction catalysts, Pt-Fe/C has been found to exhibit higher activity than Pt-Co/C as a methanol-resistant oxygen-reduction catalyst.

To prepare Pt-Fe/C and Pt-Co/C catalysts, a required amount of platinized carbon was first prepared by sulfito-complex route [74–77]. The required amount of Vulcan-XC 72R was suspended in distilled water and agitated in an ultrasonic water bath at about 80 °C to form the slurry. The desired amount of $Na_6Pt(SO_3)_4$ was dissolved in 1.0 M H_2SO_4 and diluted with distilled water, and the solution was added drop-wise to the carbon slurry with constant stirring at 80 °C. This was followed by the addition of 30% H_2O_2 with the temperature maintained at 80 °C, which resulted in vigorous gas evolution. The solution was further stirred for 1 h. Subsequently, platinized carbon was obtained by adding 1 wt.% formic acid solution, which was filtered, washed copiously with hot distilled water, and dried in an air oven at 80 °C for 2 h. Appropriate amount of Pt/C and ferric nitrate [$Fe(NO_3)_3 9H_2O$] were dispersed in a 1:1 mixture of isopropyl alcohol and Millipore water followed by its ultrasonication for about half-an-hour [78]. The *pH* of the medium was adjusted to 7 with 0.1 M solution of hydrazine and the slurry thus obtained was dried with constant stirring. The resultant mass was transferred into an alumina boat and alloyed by heating at 750 °C for 1 h under flowing hydrogen followed by annealing for 12–15 h in the same atmosphere. Pt-Co/C catalyst was prepared in a similar manner by using $Co(NO_3)_2.6H_2O$. The X-ray diffraction pattern (XRD) for Pt-Fe/C, Pt-Co/C, and Pt/C catalysts are shown in Figure 5a, b and c, respectively. The XRD patterns for Pt-Fe/C and Pt-Co/C exhibit tetragonal structures [41, 79–82], while the XRD pattern of Pt/C shown in Figure 5c could be fitted to a face-centered cubic phase [80].

Iron tetramethoxyphenylporphyrin (FeTMPP) has been reported to be the most active catalyst among transition-metal porphyrins [50, 83]. It is prepared by iron insertion into meso-tetramethoxyphenylphorphyrin ($TMPPH_2$). In brief, $TMPPH_2$ is synthesized by reaction of pyrrole with anisaldehyde in propionic acid [84]. $TMPPH_2$ thus obtained is purified by column chromatography followed by iron metal insertion with ferric chloride. The characteristic absorption spectrum of FeTMPP in benzene shows absorption maximum (λ_{max}) in the visible region between 419 and 575 nm. FeTMPP is supported on a high-surface area carbon, such as Vulcan XC-72R and is pyrolyzed at ~ 700 °C in flowing argon [48, 49]. In pyrolysed metal porphyrins, the molecular structure of the catalyst is destroyed during the heat treatment, and therefore the metal complex by default is the precursor of the actual active material. It has been proposed that the catalytic site in FeTMPP/C is N_4-Fe [50, 51] bound to the carbon support. This site has been labeled as a low-temperature catalytic site [85]. The other catalytic sites formed at elevated temperatures are not yet fully characterized. However, it is argued that the organic linkages around the iron atom help prevent its oxidation, which is seminal to its catalytic activity [85]. Metal oxides are usually prepared by a solid-state reaction of the component oxides [86] and are characterized primarily by powder XRD.

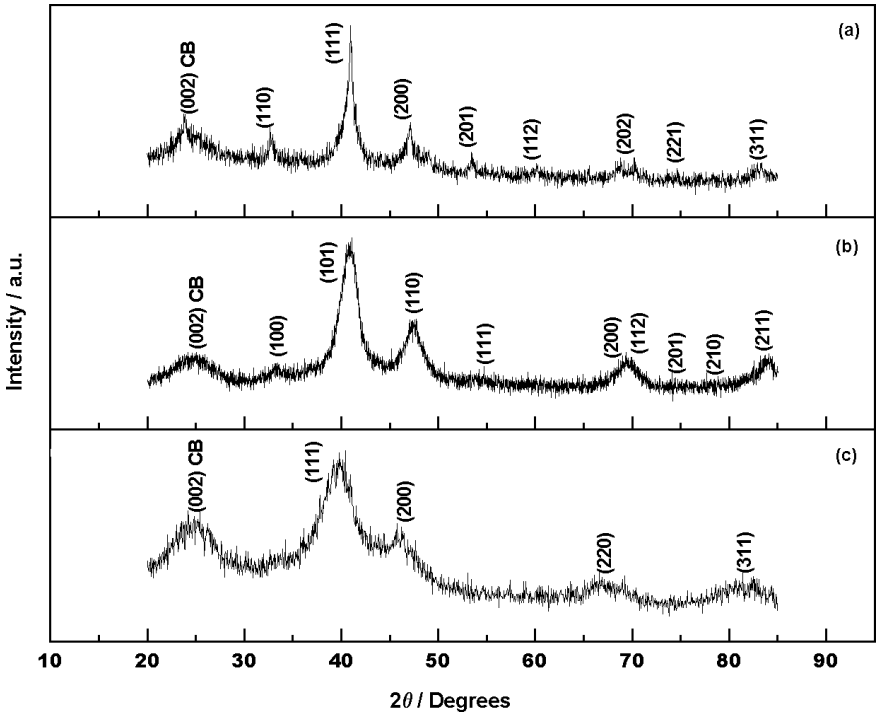

Fig. 5 X-ray powder diffraction patterns for (a) Pt-Fe/C, (b) Pt-Co/C and (c) Pt/C catalysts.

The last category of catalyst consists mainly of Ru-Mo-S, RuS, and RuSe [60, 66–68]. Among these, RuSe exhibits maximum activity as a selective oxygen-reduction catalyst. RuSe is obtained by reacting a mixture of ruthenium dodecacarbonyl [$Ru_3(CO)_{12}$] selenium at about 140 °C, with xylene in nitrogen under refluxing condition, followed by washing the resultant mass with triethyl ether [66]. These catalysts are deposited onto a Vulcan XC-72R carbon for utilization as oxygen-reduction electrodes. The powder XRD pattern for carbon-supported RuSe (RuSe/C) catalyst is given in Figure 6. This XRD pattern shows all

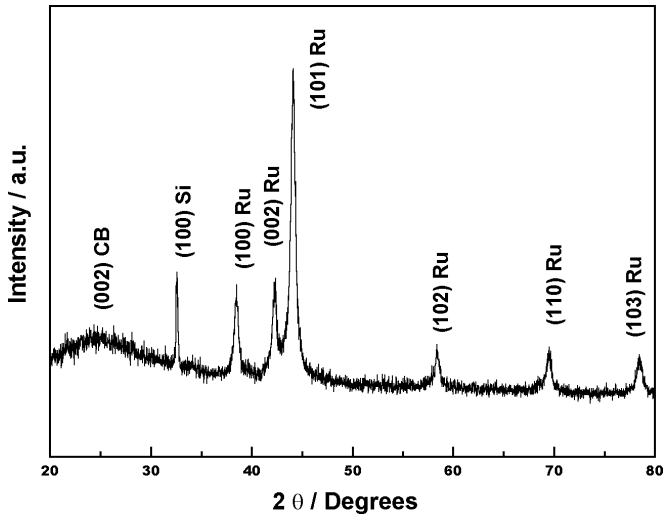

Fig. 6 X-ray powder diffraction pattern for Ru-Se/C catalyst.

characteristic peaks due to ruthenium metal, and a broad feature at the diffraction angle of $2\theta \approx 25°$ can be attributed to (002) plane of hexagonal structure of Vulcan XC-72R. The diffraction peak observed at $2\theta \approx 32°$ is due to the (100)-oriented silicon wafer, which was used as the substrate for the catalyst powder. Bron et al. [66] reported that ruthenium metal, even after refluxing in selenium-containing solution, shows little change in its XRD pattern. However, RuSe exhibits higher catalytic activity in relation to ruthenium metal. According to Bron et al., the activity enhancement by selenium is related to an interfacial effect due to the binary structure of the catalyst. Energy dispersive analysis by X-rays (EDAX) of RuSe/C catalyst suggests that the optimum quantity of selenium is ~ 15 at.% [66]. It is noteworthy that the RuSe/C catalyst is different from a metallic-ruthenium surface, and its activity towards oxygen reduction is substantially higher. Because the RuSe/C catalyst is loaded with organic matter made up of carbonyl or carboxylic groups; its high catalytic activity is probably due to an interaction of nanocrystalline ruthenium and carbon ligands. The effect can be twofold: (i) carbon species may stabilize surface ruthenium metal, thus suppressing its oxidation, which otherwise would transform ruthenium particles rapidly into RuO_2, and (ii) carbon species may alter the distribution of interfacial electronic states by forming ruthenium complexes.

A schematic description of oxygen reduction on a RuSe/C bistructural catalyst is shown in Figure 7, which depicts catalyst centers consisting of ruthenium clusters with attached carbonyl ligands [87]. Because some of the bonds are dangling (unsaturated), an interaction with oxygen can take place depending on the number of ruthenium sites available in the cluster, which act as electron-transfer mediators.

A cyclic voltammetric characterization of Pt/C, Pt-Co/C, and Pt-Fe/C catalysts in aqueous sulfuric acid, both with (Figure 8b) and without (Figure 8a) methanol, is shown in Figure 8. The data indicate that among Pt/C, Pt-Co/C, and Pt-Fe/C catalysts, the methanol oxidation reaction is least favored on the Pt-Fe/C. Therefore, Pt-Fe/C appears to be a potential selective oxygen-reduction catalyst. Pt-Fe/C has also been reported to be a potential CO-oxidation catalyst [88]. From the XPS, XAS, and cyclic voltammetric data on Pt/C and Pt-Fe/C catalysts [89], the higher oxygen-reduction activity of the Pt-Fe/C catalysts in the presence of methanol appears to be primarily due to (i) the higher proportion of active platinum sites in relation to Pt/C, and (ii) a completely different nearest neighbour environment in the Pt-Fe/C cata-

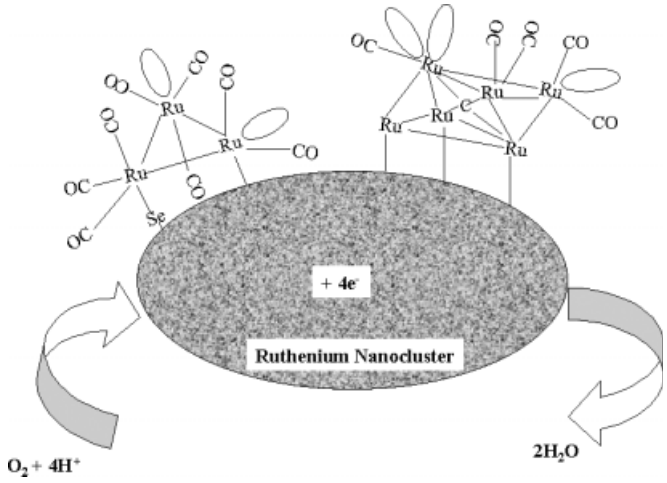

Fig. 7 Mechanism explaining the oxygen-reduction activity of Ru-Se/C catalyst.

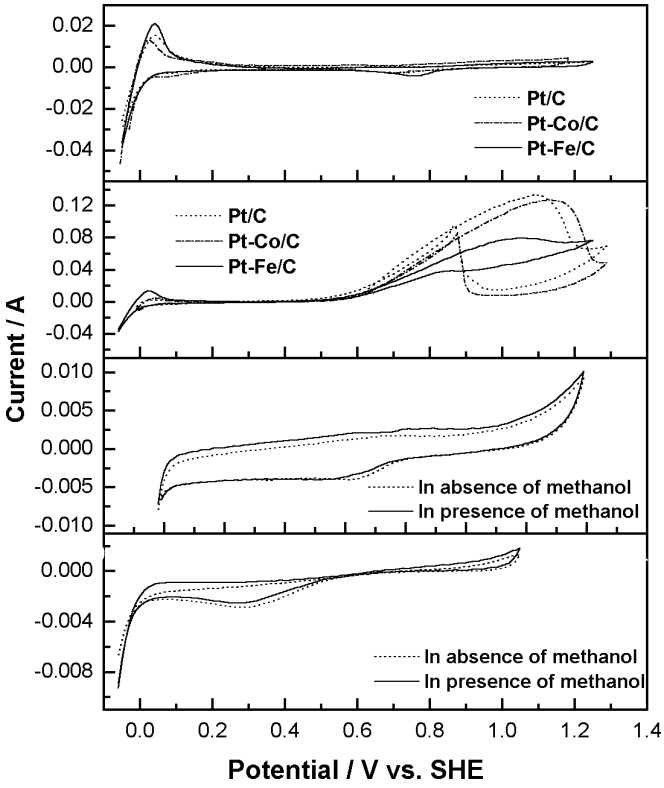

Fig. 8 Cyclic voltammograms in aqueous sulphuric acid for (a) Pt/C, Pt-Fe/C, Pt-Co/C without methanol and (b) with methanol, (c) Fe-TMPP/C catalyst with and without methanol, and (d) RuSe/C with and without methanol.

lyst where, unlike the Pt/C catalyst, the nearest neighbour sites are occupied by Fe, which helps scavenge impurities from the neighbouring active platinum sites. The cyclic voltammetric data for FeTMPP/C in sulfuric acid, with and without methanol are shown in Figure 8c [10]. These data show the methanol resistance of the catalyst towards oxygen reduction reaction. The cyclic voltammetric data for RuSe/C in sulphuric acid, with and without methanol are given in Figure 8d. Here, the data depict complete absence of methanol oxidation on RuSe/C surface. Accordingly, RuSe/C would be an effective selective catalyst for oxygen-reduction reaction.

4 Mixed-Reactant Direct Methanol Fuel Cells

In a MR-DMFC, aqueous methanol fuel and oxidant oxygen gas (or air) are mixed together before feeding to the fuel cell (Figure 3) [6, 7]. As indicated in Table 1, there is no need for gas-tight structure within the MR-DMFC stack providing relaxation for sealing of reactants/products delivery structure.

The galvanostatic polarization data for the selective reactants and mixed-reactants anode tests are given in Figure 9a and b, respectively [9]. There was no significant difference between the polarization data of the mixed-feed anode with methanol plus air and mixed-feed anode with methanol plus nitrogen, which is in accord with the findings of Barton et al. [6]. This suggests that there was no parasitic oxidation of methanol with oxygen in the air in the MR-DMFC. The small difference in the anode polarization data during the selective-reactants and mixed-reactants anode test seen in the mass-polarization region was possibly because the mixed-feed helped scavenging carbon dioxide from the catalytic sites ameliorating oxidation of methanol at the anode [8]. It is noteworthy that a DMFC operating at 1.0 A load would require 7.06×10^{-8} dm^3 s^{-1} of liquid methanol at the anode, and will result in a CO_2 exhaust of 3.87×10^{-5} dm^3 s^{-1} (if present as gas) at its anode. This represents about 550-fold volume increase in the anode compartment of the cell during its operation and suggests that CO_2 removal from the anode should improve the cell performance.

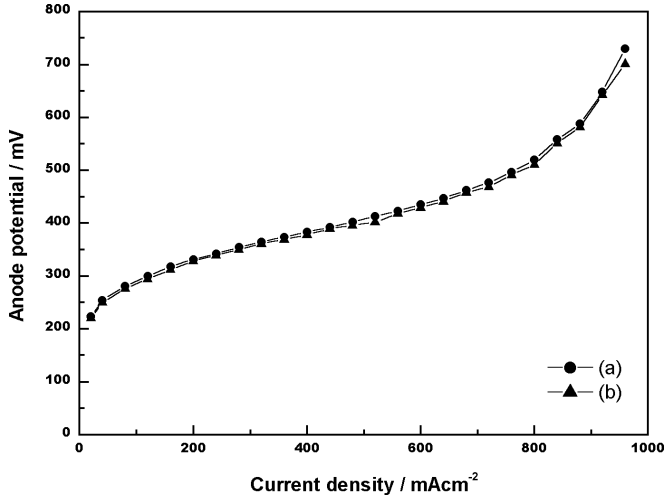

Fig. 9 Polarization data obtained at 90 °C for (a) selective-reactant anode, and (b) mixed-reactant anode.

The cathode polarization curves for oxygen-reduction using Pt/C, Pt-Co/C and Pt-Fe/C catalysts obtained by oxidizing hydrogen at the anode, which also acts as the reference electrode, are shown in Figure 10c. These data show superior performance for the Pt/C cathode. But as the methanol is passed over the anode, a lower cell performance was found for the cell employing the Pt/C catalyst in relation to both Pt-Co/C and Pt-Fe/C cathodes (Figure 10a) [10]. This clearly reflects the chemisorption of methanolic residues over Pt/C cathode by methanol crossover from anode to cathode, which leads to increased overpotential for oxygen reduction. The anode performance was similar for all the cells tested, as shown in Figure 10b. The Pt-Co/C catalyst exhibits a performance better than that of Pt/C catalyst but is inferior to the Pt-Fe/C catalyst [10]. These data clearly suggest Pt-Fe/C to be an effective selective oxygen-reduction catalyst and corroborate the cyclic voltammetry data on Pt/C, Pt-Co/C, and Pt-Fe/C presented in Figure 8.

In MR-DMFCs, cathode selectivity is paramount and is accomplished by using oxygen-reduction catalysts, which in addition to being tolerant to methanol, do not oxidize it [48,

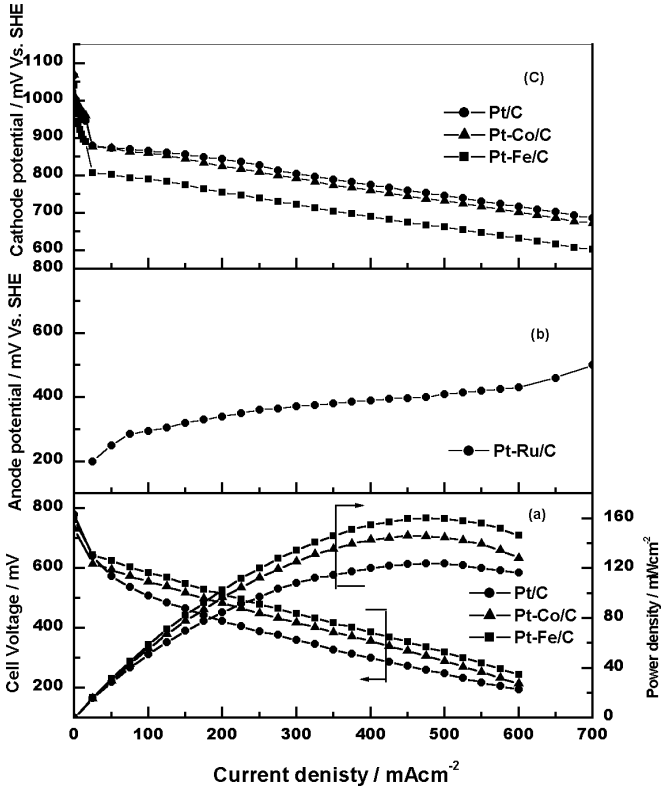

Fig. 10 (a) Polarization data for a MR-DMFC at 90 °C comprising Pt-Ru/C (1:1) anode with a Pt loading of 2.5 mg cm^{-2} and a Pt/C, Pt-Co/C (1:1) or Pt-Fe/C (1:1) cathode with a Pt loading of 1.37 mg cm^{-2}. The individual anode and cathode data for the MR-DMFCs are shown in (b) and (c), respectively.

49, 57–68, 90–94]. The performance characteristics of certain MR-DMFCs, employing various methanol-resistant oxygen-reduction catalysts at the cathode and a Pt-Ru/C catalyst at the anode, are shown in Figures 11 and 12 [9]. The performance curves at 90 °C for the MR-DMFCs employing 1.0 mg cm^{-2} of FeTMPP/C, CoTMPP/C, FeCoTMPP/C, and RuSe/C at the cathode are shown in Figure 11. Among these, the best performance, with a maximum power output of ~ 30mW cm^{-2}, is observed for the MR-DMFC employing 1 mg cm^{-2} of RuSe/C catalyst at the cathode. The performance curves at 90 °C for the mixed-reactants DMFCs employing varying amounts of RuSe/C at the cathode are shown in Figure 12. It is found that the best performance at the maximum output power of about 50 mW cm^{-2} is obtained

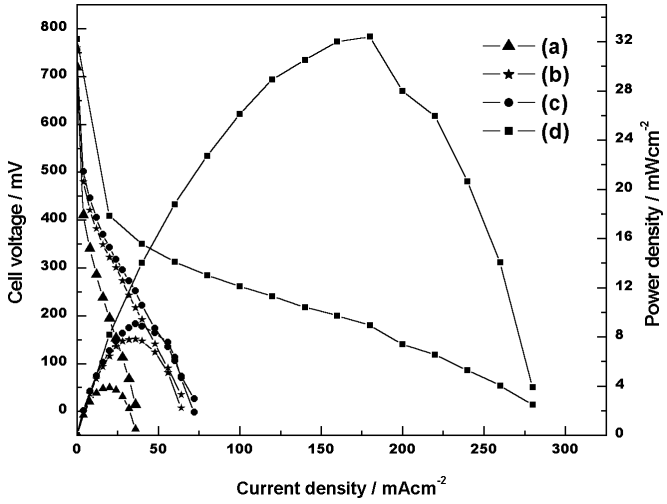

Fig. 11 Performance data for MR-DMFCs with Pt-Ru/C anode and cathode comprising (a) Co-TMPP/C, (b) FeCo-TMPP/C, (c) Fe-TMPP/C, and (d) RuSe/C catalysts.

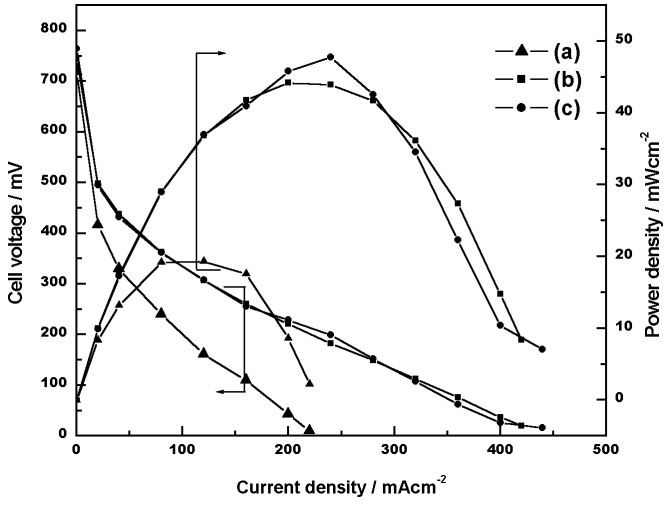

Fig. 12 Performance data for MR-DMFCs with Pt-Ru/C anode and cathode with (a) 1 mg cm^{-2}, (b) 2 mg cm^{-2}, and (c) 2.5 mg cm^{-2} of RuSe/C.

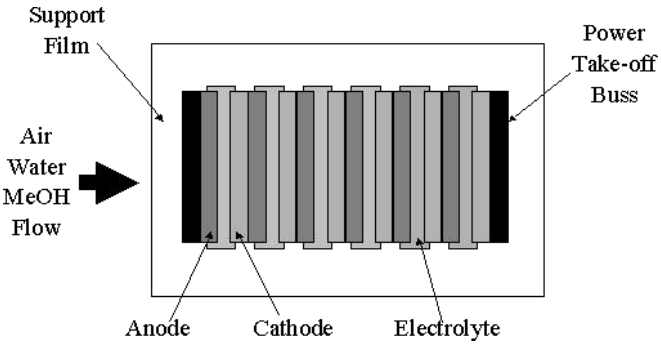

Fig. 13 Schematic diagram of a MR-DMFC with strip-electrode design.

for the MR-DMFC with the RuSe/C loading of 2.5 mg cm^{-2}, while operating the MR-DMFC with methanol plus oxygen. A maximum output power of ~ 20 mW cm^{-2} is obtained when operating the cell with methanol plus air.

Recently, researchers from IFC and UT-Austin have demonstrated that the performance of a MR-DMFC with selective electrodes could exceed that of the CDMFCs when the fuel and the oxidant are supplied at identical rates to the anode and the cathode, respectively [6]. They also conducted a design study in which the dimensions of a series of mixed-reactants, strip cell DMFCs were optimized (Figure 13). In the single cell tests, a two-phase reactant mixture of 1.0 M methanol (3 ml min^{-1}) and air (3 l min^{-1}) was supplied to both sides of a conventional geometry membrane electrode assembly at 80 °C. The 32 cm^2 MEA consisted of a Nafion®-117 membrane coated on one side with a hydrophobic Pt-Ru/C (5 mg cm^{-2}) anode, and on the other side with iron tetra-methoxy phenylporphyrin (FeTMPP), a methanol-tolerant cathode material. The half-cell experiments demonstrated that, in the system, there was little reaction between oxygen and methanol at the anode and that the main effect of the entrained air or nitrogen in the mixed-feed was to impede mass transport of the feed to the anode at current densities above 100 mA cm^{-2}. At the cathode, half-cell measurements again showed little difference while operating in mixed-reactant and conventional separated-reactant modes. Consequently, performance of the SPE-DMFCs in mixed-reactant mode was identical to the performance of SPE-DMFCs in conventional mode. In the MR-DMFCs, one may argue that methanol crossover does not affect the cathode performance, a situation quite opposite to CDMFCs. In the latter, methanol leaks constantly from the anode to the cathode causing both a lowering in its potential and wastage of fuel through direct chemical oxidation.

Mixing a fuel and oxidant within the fuel cell raises immediate concerns of potential explosion. However, in reality, a fuel cell stack largely filled with electrolyte, electrode and separator materials, which acts as heat sink and eliminates the possibility of explosion. Indeed, MR-SOFCs, which operate at high temperatures, support the safety view in the mixed-reactants fuel cell systems.

5 Conclusions

MRFC technology offers immediate benefits in cost, size, power density and reliability with increased fuel efficiency. In the future, with the development of efficient selective electrocatalysts, MRFCs could replace conventional, separated-reactant fuel cells in several application areas.

References

[1] J. Larminie, A. Dicks, *Fuel Cell Systems Explained*, Wiley, New York, **2000**.
[2] K. Kordesch, G. Simader, *Fuel cells and Their Applications*, Wiley-VCH, Weinheim, **1994**.
[3] A. Hamnett, *Philos. Trans. R. Soc. London Ser.* **1996**, *A354*, 1653.
[4] A. S. Aricò, S. Srinivasan, V. Antonucci, *Fuel Cells* **2001**, *1*, 1.
[5] V. Klouz, V. Fierro, P. Denton, H. Katz, J. P. Lisse, S. Bouvot-Mauduit, C. Mirodatos, *J. Power Sources* **2002**, *105*, 26.
[6] S. C. Barton, T. Patterson, E. Wang, T. F. Fuller, A. C. West, *J. Power Sources* **2001**, *96*, 329.
[7] M. A. Priestnall, V. P. Kotzeva, D. J. Fish, E. M. Nilsson, *J. Power Sources* **2002**, *106*, 21.
[8] A. K. Shukla, C. L. Jackson, K. Scott, G. Murgia, *J. Power Sources* **2002**, *111*, 43.
[9] K. Scott, A. K. Shukla, C. L. Jackson, W. R. A. Meuleman, *J. Power Sources* **2004**, *126*, 67.
[10] A. K. Shukla, R. K. Raman, *Annu. Rev. Mater. Res.* **2003**, *33*, 155.
[11] P. G. Grimes, B. Fielder, J. Adam, *Proc. Annual Power Sources Conf.* **1961**, *15*, 29.
[12] G. Grunenberg, W. Wicke, E. Justi, *Br. Patent GB 994448*, **1961**.
[13] G. Goebel, B. D. Struck, W. Vielstich in *Fuel Cells – Modern processes for the electrochemical production of energy*. W Vielstich, Wiley Intersciene, Germany, **1965**.
[14] W. van Gool, *Philps Res. Reports* **1965**, *20*, 81.
[15] G. A. Louis, J. M. Lee, D. L. Maricle, J. C. Tocciola, *US Patnet 4248941*, **1981**.
[16] C. K. Dyer, *Nature* **1990**, *343*, 547.
[17] T. Hibino, H. Iwahara, *Chem. Letts.* **1993**, 1131.
[18] I. Riess, P. J. van der Put, J. Schoonman, *Solid State Ionics* **1995**, *82*, 1.
[19] T. Hibino, K. Asano, H. Iwahara, *Nippon Kagaku Kaishi* **1994**, *7*, 600.
[20] T. Hibino, A. Hashimoto, T. Inoue, J. I. Tokuno, S. I. Toshida, M. Sano, *Science* **2000**, *288*, 2031.
[21] T. Hibino, K. Ushiki, Y. Kuwahara, *Japanese Patnet JP 02910977 B2*, **1995/98**.
[22] M. Joerger, *joint meeting of the 192nd Electrochem Soc. Meeting and 48th Annual Meeting of the Int. Soc. Of Electrichem*, Paris.
[23] K. Asano, T. Hibino, H. Iwahara. *J. Electrochem. Soc.* **1995**, *142*, 3241.
[24] T. Hibino, A. Hashimoto, T. Inoue, J. I. Tokuno, S. I. Toshida, M. Sano, *J. Electrochem. Soc.* **2000**, *147*, 2888.
[25] A. K. Shukla, C. L. Jackson, K. Scott, R. K. Raman, *Electrochim. Acta* **2002**, *47*, 3401.
[26] N. Munichandraiah, K. McGrath, G. K. S. Prakash, R. Aniszfeld, G. A. Olah, *J. Power Sources* **2003**, *117*, 98.
[27] B. Gurau, E. S. Smotkin, *J. Power Sources* **2002**, *112*, 339.
[28] A. Heinzel, V. M. Barragán, *J. Power Sources* **1999**, *84*, 70.
[29] P. S. Kauranen, E. Skou, J. Munk, *J. Electroanal. Chem.* **1996**, *404*, 1.
[30] V. S. Bagotzky, Y. B. Vassilyer, *Electrochim. Acta* **1967**, *12*, 1323.
[31] W. H. Lizcano-Valbuena, V. A. Paganin, E. R. Gonzalez, *Electrochim. Acta* **2002**, *47*, 3715.
[32] K. L. Ley, R. Liu, C. Pu, Q. Fan, N. Leyarovska, C. Serge, E. S. Smotkin, *J. Electrochem. Soc.* **1997**, *144*, 1543.
[33] E. Herrero, W. Chrzanowski, A. Wieckowoski, *J. Phys. Chem.* **1995**, *99*, 10423.
[34] A. K. Shukla, M. K. Ravikumar, A. S. Aricò, G. Candiano, V. Antonucci, N. Giordano, A. Hamnett, *J. Appl. Electrochem.* **1995**, *25*, 528.
[35] A. S. Aricò, H. Kim, V. Antonucci, A. K. Shukla, M. K. Ravikumar, N. Giordano, *Electrochim. Acta* **1994**, *39*, 691.
[36] A. S. Aricò, V. Antonucci, N. Giordano, A. K. Shukla, M. K. Ravikumar, A. Roy, S. R. Barman, D. D. Sarma, *J. Power Sources* **1994**, *50*, 295.
[37] M. Watanabe et al, *J. Electroanal. Chem.* **1987**, *229*, 395.
[38] L. Mao, K. Arihara, T. Sotomura, T. Ohsaka, *Chem. Commun.* **2003**, *22*, 2818.
[39] N. M. Marković, T. J. Schmidt, V. Stamenković, P. N. Ross, *Fuel Cells* **2001**, *1*, 105.
[40] L. Geines, R. Faure, R. Durand, *Electrochim. Acta* **1998**, *44*, 1317.
[41] T. Toda, H. Igarashi, H. Uchida, M. Watanabe, *J. Electrochem. Soc.* **1999**, *146*, 3750.
[42] T. Toda, H. Igarashi, M. Watanabe, *J. Electrochem. Soc.* **1998**, *145*, 4185.
[43] S. Mukerjee, S. Srinivasan, M. P. Soriaga, J. McBreen, *J. Electrochem. Soc.* **1995**, *142*, 1409.
[44] S. Mukerjee, S. Srinivasan, M. P. Soriaga, J. McBreen, *J. Phys. Chem.* **1995**, *99*, 4577.
[45] S. Štrbac, R. R. Adžič, *J. Electroanal. Chem.* **1996**, *403*, 169.
[46] S. Štrbac, N. A. Anastasijevic, R. R. Adžič, *Electrochim. Acta* **1994**, *39*, 983.
[47] R. Jasinski, *J. Electrochem. Soc.* **1965**, *112*, 526.
[48] G. Q. Sun, J. T. Wang, R. F. Savinell, *J. Appl. Electrochem.* **1998**, *28*, 1087.
[49] S.Gupta, D. Tryk, S. K. Zecevic, W. Aldred, D. Guo, R. F. Savinell, *J. Appl. Electrochem.* **1998**, *28*, 673.
[50] S. L. J. Gojković, S. Gupta, R. F. Savinell, *J. Electroanal. Chem.* **1999**, *462*, 63.
[51] H. Kalvelage, A. Mecklenburg, U. Kunz, U. Hoffmann, *Chem. Eng. Technol.* **2000**, *23*, 803.
[52] J. B. Goodenough, *Prog. Solid State Chem.* **1971**, *5*, 39.
[53] S. Trassatti, *Electrodes of Conducting Metallic Oxides, Part B*, Elsevier, Amsterdam, **1981**.

[54] M. R. Tarasevich, B. N. Efremov, *Electrodes of Conducting Metallic Oxides, Part A*, (Ed. S. Trassatti), Elsevier, Amsterdam, **1981**, pp. 221.
[55] H. Tamura, H. Yoneyama, Y. Matsumoto, *Electrodes of Conducting Metallic Oxides, Part A*, (Ed. S. Trassatti), Elsevier, Amsterdam, **1981**, pp. 261.
[56] J. B. Goodenough, A. K. Shukla, C. Paliterio, K. R. Jamieson, A. Hamnett, R. Manoharan, *Br. Patent No. 8422546*, **1985**.
[57] V. Trapp, P. Christensen, A. Hamnett, *Faraday Trans.* **1996**, *92*, 4311.
[58] C. Fischer, N. Alonso-Vante, S. Fiechter, H. Tributsch, *J. Appl. Electrochem.* **1995**, *25*, 1004.
[59] R. W. Reeve, P. A. Christensen, A. Hamnett, S. A. Haydock, S. C. Roy, *J. Electrochem. Soc.* **1998**, *145*, 3463.
[60] P. J. Sebastian, F. J. Rodriguez, O. Solorza, R. Rivera, *J. New Mater. Electrochem. Syst.* **1999**, *2*, 115.
[61] O. Solorza-Feria, S. Citalán-Cigarroa, R. Rivera-Noriega, S. M. Fernández-Valverde, *Electrochem. Commun.* **1999**, *1*, 585.
[62] S. Durón, R. Rivera-Noriega, M. A. Leyva, P. Nkeng, G. Poillerat, O. Solorza-Feria, *J. Solid State Electrochem.* **2000**, *4*, 70.
[63] S. Durón, R. Rivera-Noriega, G. Poillerat, O. Solorza-Feria, *J. New Mater. Electrochem. Syst.* **2001**, *4*, 17.
[64] F. J. Rodriguez, P. J. Sebastian, *Int. J. Hydrogen Energy* **2000**, *25*, 243.
[65] N. Alanso-Vante, P. Bogdanoff, H. Tributsch, *J. Catalysis* **2000**, *190*, 240.
[66] M. Bron, P. Bogdanoff, S. Fiechter, I. Dorbandt, M. Hilgendorff, et al., *J. Electroanal. Chem.* **2001**, *500*, 510.
[67] V. Le Rhan, N. Alonso-Vante, *J. New Mater. Electrochem. Syst.* **2000**, *3*, 331.
[68] H. Tributsch, M. Bron, M. Hilgendorff, H. Schulenburg, I. Dorbandt, et al., *J. Appl. Electrochem.* **2001**, *31*, 739.
[69] N. Alonso-Vante, B. Schubert, H. Tributsch, *Mater. Chem. Phys.* **1989**, *22*, 281.
[70] H. G. Petrow, R. J. Allen, *U. S. Patent No. 3992331*, **1976**.
[71] H. Bönnemann, W. Brijoux, *Angew. Chem. Int. Ed. Engl.* **1991**, *30*, 1312.
[72] H. Bönnemann, P. Britz, U. Endruschat, R. Mörtel, et al., *J. New Mater. Electrochem. Syst.* **2000**, *3*, 199.
[73] F. Maillard, M. Martin, F. Gloaguen, J. M. Léger, *Electrochim. Acta* **2002**, *47*, 3431.
[74] M. K. Ravikumar, A. K. Shukla, *J. Electrochem. Soc.* **1996**, *143*, 2601.
[75] H. G. Petrow, R. J. Allen, *US Patent 3992331*, **1976**.
[76] H. G. Petrow, R. J. Allen, *US Patent 3992512*, **1976**.
[77] H. G. Petrow, R. J. Allen, *US Patent 4044193*, **1975**.
[78] Z. Wei, H. Guo, Z. Tang, *J. Power Sources* **1996**, *62*, 233.
[79] S. Sun, C. B. Murray, D. Weller, L. Folks, A. Moser, *Science* **2000**, *287*, 1989.
[80] A. K. Shukla, M. Neergat, P. Bera, V. Jayaram, M. S. Hegde, *J. Electroanal. Chem.* **2001**, *504*, 111.
[81] M. Neergat, A. K. Shukla, K. S. Gandhi, *J. Appl. Electrochem.* **2001**, *31*, 373.
[82] S. Mukerjee, S. Srinivasan, *J. Electroanal. Chem.* **1993**, *357*, 201.
[83] D. Chu, R. Jiang, *U. S. Patent No. 6245707*, **2001**.
[84] P. Stevens, A. K. Shukla, A. Hamnett, *I. Chem. E. Symp. Ser.* **1989**, *112*, 141.
[85] M. Bron, S. Fiechter, M. Hilgendroff, P. Bogdanoff, *J. Appl. Electrochem.* **2002**, *32*, 11.
[86] P. Hagenmuller, *Preparative Methods in Solid State Chemistry*, Academic, New York, **1972**.
[87] P. Bogdanoff, S. Fiechter, H. Tributsch, M. Bron, I. Dorbandt, et al., *Ger. Patent 10035841-A1*, **1999**.
[88] H. Uchida, H. Ozuka, M. Watanabe, *Electrochim. Acta* **2002**, *47*, 3629.
[89] A. K. Shukla, R. K. Raman, N. A. Choudhury, K. R. Priolkar, P. R. Sarode, S. Emura, R. Kumashiro, *J. Electroanal. Chem.* **2004**, *563*, 181.
[90] S. Popovici, W. Leyffer, R. Holze, *J. Porphyrins Phthalocyanines* **1998**, *2*, 249.
[91] T. Okada, M. Yoshida, T. Hirose, K. Kasuga, T. Yu, et al., *Electrochim Acta* **2000**, *45*, 4419.
[92] G. Q. Sun, J.-T. Wang, S. Gupta, R. F. Savinell, *J. Appl. Electrochem.* **2001**, *31*, 1025.
[93] P. Convert, C. Coutanceau, P. Crouïgneau, F. Gloaguen, C. Lamy, *J. Appl. Electrochem.* **2001**, *31*, 945.
[94] D. Chu, R. Jiang, *Solid State Ionics* **2002**, *148*, 591.

